Composite Structures 250 (2020) 112546

Contents lists available at ScienceDirect

Composite Structures

journal homepage: www.elsevier.com/locate/compstruct

Micromechanical analysis of transversal strength of composite laminae

Lucas L. Vignoli [a,b], Marcelo A. Savi [a], Pedro M.C.L. Pacheco [c], Alexander L. Kalamkarov [d,*]

[a] Center for Nonlinear Mechanics, COPPE – Department of Mechanical Engineering, Universidade Federal do Rio de Janeiro, P.O. Box 68.503, 21.941.972 Rio de Janeiro, Brazil
[b] Center for Technology and Application of Composite Materials, Department of Mechanical Engineering, Universidade Federal do Rio de Janeiro, Macaé, RJ, Brazil
[c] Department of Mechanical Engineering, Centro Federal de Educação Tecnológica Celso Suckow da Fonseca CEFET/RJ, Rio de Janeiro, RJ, Brazil
[d] Department of Mechanical Engineering, Dalhousie University, Halifax, Nova Scotia B3H 4R2, Canada

ARTICLE INFO

Keywords:
Composite material
Unidirectional laminae
Micromechanics
Analytical modeling
Transversal tensile
Compressive and shear strengths

ABSTRACT

The paper presents analysis of several micromechanical models for estimating transversal strength of composite laminae and comparing theoretical results with the available experimental data. The tensile, compressive and shear transversal strengths are analyzed. For a load transversal to the fiber direction, micromechanical analysis becomes complicated due to stress concentration. In order to deal with it, an elasticity-based solution is used to obtain stress around single inclusion in infinite matrix. In addition, the finite element simulations are carried out to derive approximation functions for actual values of fiber volume fraction. For tensile transversal strength, the density of dilatational energy is assumed to be the dominant failure mechanism, while for the compressive transversal strength, the interface failure is modeled. Since the critical dilatational energy and interface strength are commonly unavailable in literature, average values are obtained based on the experimental data. Alternatively, a semi-empirical modification of Chamis model is also proposed. For transversal shear strength, the results indicate that the matrix shear strength provides a good approximation. It should be noted that closed-form expressions are obtained, resulting in simple and efficient implementation for engineering applications and design optimization. Results are compared with other micromechanical models and with 58 experimental data from the literature. In general, elasticity-based models and modified Chamis model present a considerable advancement in transversal strength estimation with the small average errors.

1. Introduction

Due to the absence of reliance of failure predictions, the international effort namely Word Wide Failure Exercise (WWFE) was established in order to define proper approaches for composite material design [1]. WWFE's participants have been able to present a great advance about failure criteria for unidirectional composites. However, to properly predict laminate strengths a previous step must be regarded that is out of WWFE's scope: micromechanical modeling.

Numerical modeling of unidirectional laminae [4,5] is a natural approach to deal with micromechanical analysis. The essential idea is to define a representative volume element (RVE) that allows the analysis of the whole structure. Despite some recent contributions, there are two main drawbacks in this approach: the difficulty of the RVE definition; and the computational cost. Wongsto & Li [6] pointed out the influence of RVE on the results of numerical simulations, concluding that it must be large enough to provide an adequate representation of the structure. The random pattern of distribution is unavoidable due to manufacturing issues and, based on this, Elnekhaily & Talreja [7] established a convergence analysis to define RVE that must contain 576 fibers.

Composite design optimization considering micromechanical aspects (fibers, matrices and constituents' volume fractions), becomes prohibitive by considering the need to generate RVE with 576 fibers to simulate each combination. As discussed by Andrianov *et al.* [8], analytical formulations have the great advantage of simple implementation and computation for structural optimization. Tsai & Melo [9] highlighted that the large number of variables involved in composite design indicates the advantage of the use of analytical approaches.

This emphasizes significance of micromechanical analytical analysis in composite material design. Vignoli *et al.* [2] presented a critical overview of analytical models for the elastic properties. Nevertheless, very few analytical models are found in the literature for transversal strengths. The simplest one assumes that transversal strengths are highly influenced by the perturbation on the stress field around the fibers [10]. The most popular is the Chamis model [11], which consid-

* Corresponding author.
E-mail addresses: ll.vignoli@mecanica.coppe.ufrj.br (L.L. Vignoli), savi@mecanica.ufrj.br (M.A. Savi), pedro.pacheco@cefet-rj.br (P.M.C.L. Pacheco), alex.kalamkarov@dal.ca (A.L. Kalamkarov).

https://doi.org/10.1016/j.compstruct.2020.112546
Received 11 March 2020; Revised 7 May 2020; Accepted 26 May 2020
Available online 18 June 2020
0263-8223/© 2020 Elsevier Ltd. All rights reserved.

ers a simplified RVE assuming a square fiber. The most recent model for transversal strength is the Bridging model [12] that is based on the concentric cylinder modeling. It should be pointed out that these analytical models for transversal strengths of unidirectional laminae present a poor prediction comparing with the experimental data [3], which makes the present micromechanical analysis relevant and essential for composite material design.

This paper deals with micromechanical models to estimate transversal strength of unidirectional composite laminates. Based on a macromechanical perspective, six strength properties are required based on the coordinate system shown in Fig. 1, where the direction x_1 coincides to the direction of fibers and the plane $x_2 - x_3$ is transversal to the fibers: longitudinal tension, S_{11}^t; longitudinal compression, S_{11}^c; transversal tension, S_{22}^t; transversal compression, S_{22}^c; longitudinal shear, S_{12}^s; and transversal shear, S_{23}^s. Note that distribution of fibers is assumed to be symmetrical in plane $x_2 - x_3$, and therefore, the lamina is transversally isotropic with $S_{12}^s = S_{13}^s$, $S_{22}^t = S_{33}^t$ and $S_{22}^c = S_{33}^c$.

The objective of the present investigation is to evaluate transversal strengths S_{22}^t, S_{22}^c and S_{23}^s. The estimation of these transversal properties is a big micromechanics challenge due to a number of issues, as for example: fiber non-uniform arrangement [8], thickness effect [13], and interface properties [3]. Consequently, it is expected that the estimation of these three strengths needs more information than the ones based only on the properties of constituents.

The developed analysis assumes that the constituent properties are input information, in agreement with the World Wide Failure Exercise (WWFE) – see the guidelines in references [14,15]. Based on that, the following constituents are considered for the estimation of transversal strength: fiber longitudinal and transversal elastic moduli, E_1^f and E_2^f; fiber longitudinal and transversal shear moduli, G_{12}^f and G_{23}^f; fiber longitudinal Poisson's ratio, ν_{12}^f; fiber tensile and compressive strengths, S_t^f and S_c^f; matrix elastic modulus, E^m; matrix Poisson's ratio, ν^m; matrix tensile, compressive and shear strengths, S_t^m, S_c^m and S_s^m. However, the transversal load may require some additional properties, as the critical dilatational energy and the interface strength. Since these properties are usually unknowns, an investigation about the reasonable average values is carried out.

After this introduction, the paper is organized as follows. In Section 2, the main micromechanical models available in the literature are reviewed, and a novel model is proposed based on a modification of the Chamis model. An elasticity-based set of equations are derived in the Section 3 using finite element simulation to obtain approximate functions, establishing the closed-form equations. Results are presented and discussed in Section 4. Finally, the conclusions are highlighted in Section 5.

2. Classical analytical models

A brief review of the main existing analytical models are presented in this Section, namely the Rule of Mixture with Stress Concentration (ROM-Kt), Chamis (Ch) and Bridging (Br). A novel modified version of the Chamis model is also proposed.

2.1. Rule of Mixture with stress concentration (ROM-Kt)

When a transversal load is applied in a lamina, stress concentration effects are induced due to fibers distribution in the matrix. Based on this observation, many textbooks [10,16,17] suggest the use of the classical Rule of Mixture as basis, considering that fibers and matrix work like elements in series when subjected to transversal loads, which means that all the constituents have the same load. Accounting for the stress concentration factor, the following equations are obtained:

$$S_{22}^t = \frac{S_t^m}{K_\sigma} \tag{1}$$

$$S_{22}^c = \frac{S_c^m}{K_\sigma} \tag{2}$$

where S_t^m and S_c^m are the matrix tensile and compressive strengths, respectively, and K_σ is the stress concentration factor defined by

$$K_\sigma = \frac{1 - V_f[1 - (E^m/E_2^f)]}{1 - (4V_f/\pi)^{0.5}[1 - (E^m/E_2^f)]} \tag{3}$$

where E^m is the matrix elastic modulus, E_2^f is the fiber transverse elastic modulus and V_f is the fiber volume fraction.

2.2. Chamis model (Ch)

Devireddy & Biswas [18] presented a numerical study comparing effective elastic and thermal properties of unidirectional composites assuming fibers with square cross section. Results indicate very close effective properties when compared with numerical simulation considering fibers with circular cross section. Accordingly, the RVE with square fiber is shown in Fig. 2.

The RVE has $V_f = (a/b)^2$, where a and b are the sizes of fiber and RVE, respectively, and it is divided in 5 parts: the sub-cells 2i, 2ii and 2iii work in series to build a cell 2, that is parallel to cells 1 and 3. Sub-cells 1, 2i, 2iii and 3 are the matrix and 2ii is the fiber. The equilibrium requirements are defined by

$$\sigma_{22}a^2 = \sigma_{22}^{(1)}a\left(\frac{a-b}{2}\right) + \sigma_{22}^{(2)}ab + \sigma_{22}^{(3)}a\left(\frac{a-b}{2}\right) \tag{4}$$

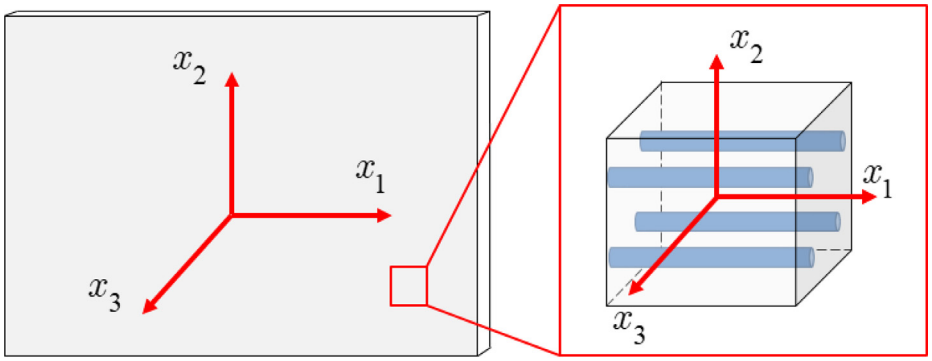

Fig. 1. Definition of coordinate systems used to define the materials properties.

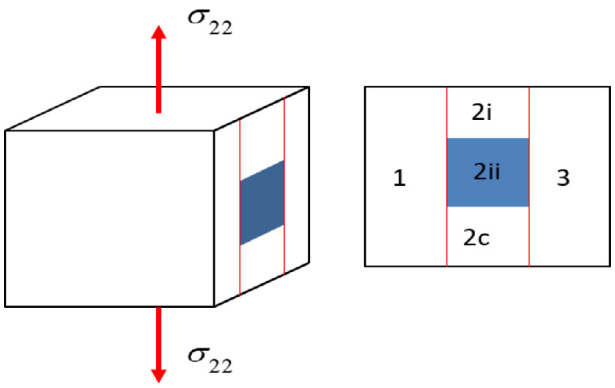

Fig. 2. RVE with square fiber subjected to transversal tensile load.

$$\sigma_{22}^{(2)} = \sigma_{22}^{(2i)} = \sigma_{22}^{(2ii)} = \sigma_{22}^{(2iii)} \tag{5}$$

From the geometrical compatibility,

$$\varepsilon_{22}^{(1)} = \varepsilon_{22}^{(2)} = \varepsilon_{22}^{(3)} \tag{6}$$

$$\varepsilon_{22}^{(2)} = \varepsilon_{22}^{(2i)}\left(\frac{1-\sqrt{V_f}}{2}\right) + \varepsilon_{22}^{(2ii)}\sqrt{V_f} + \varepsilon_{22}^{(2iii)}\left(\frac{1-\sqrt{V_f}}{2}\right) \tag{7}$$

Using linear elastic constitutive relation for both constituents, the relations for stresses in each sub-cell can be obtained, and the relation between the applied stress, σ_{22}, and the stress in each component can be computed using Eq. (4). For tensile load, assuming that the failure is defined by the conditions $\sigma_{22}^{(2i)} = \sigma_{22}^{(2iii)} = S_t^m$ and $\sigma_{22} = S_{22}^t$, the transversal tensile strength can be estimated by

$$S_{22}^t = \left[1 - \left(\sqrt{V_f} - V_f\right)\left(1 - \frac{E^m}{E_2^f}\right)\right] S_t^m \tag{8}$$

Chamis model [11] used Eq. (9) as the basis, but also included the effect of voids, suggesting the following equation:

$$S_{22}^t = \left[1 - \left(\sqrt{V_f} - V_f\right)\left(1 - \frac{E^m}{E_2^f}\right)\right]\left[1 - \sqrt{\frac{4V_v}{\pi(1-V_f)}}\right] S_t^m \tag{9}$$

where V_v is the volume fraction of voids.

The same procedure can be carried out for compressive strength, resulting in the following equation:

$$S_{22}^c = \left[1 - \left(\sqrt{V_f} - V_f\right)\left(1 - \frac{E^m}{E_2^f}\right)\right]\left[1 - \sqrt{\frac{4V_v}{\pi(1-V_f)}}\right] S_c^m \tag{10}$$

For transversal shear strength, Chamis model defines

$$S_{23}^s = \left[\frac{1 - \sqrt{V_f}\left(1 - \frac{G^m}{G_{23}^f}\right)}{1 - V_f\left(1 - \frac{G^m}{G_{23}^f}\right)}\right] S_s^m \tag{11}$$

where S_s^m is the matrix shear strength.

Using Eq.(8) as basis, the following modified version of Chamis model is proposed to improve the estimations

$$S_{22}^t = \left[1 - \left(\sqrt{V_f} - V_f\right)\left(1 - \frac{E^m}{E_2^f}\right)\right]^{n_t} S_t^m \tag{12}$$

$$S_{22}^c = \left[1 - \left(\sqrt{V_f} - V_f\right)\left(1 - \frac{E^m}{E_2^f}\right)\right]^{n_c} S_c^m \tag{13}$$

where n_t and n_c are calibrated in the Section 4 according to the compiled experimental data.

2.3. Bridging model (Br)

For transversal strengths, the Bridging model assumes that the matrix is associated with the plane strain conditions and proposes the modeling of the stress concentration effect around the fiber from the micromechanical point of view. Using the Coulomb-Mohr criterion to define the matrix failure, the transversal strengths are estimated by

$$S_{22}^t = \left[V_f \frac{E_2^f}{(\beta E_2^f + (1-\beta)E^m)} + (1 - V_f)\right] \frac{S_t^m}{k_{22}^t} \tag{14}$$

$$S_{22}^c = \left[V_f \frac{E_2^f}{(\beta E_2^f + (1-\beta)E^m)} + (1 - V_f)\right] \frac{S_c^m}{k_{22}^c} \tag{15}$$

$$S_{23}^s = \left[V_f \frac{E_2^f}{(\beta E_2^f + (1-\beta)E^m)} + (1 - V_f)\right] \left(\frac{k_{22}^c}{S_c^m} + \frac{k_{22}^t}{S_t^m}\right)^{-1} \tag{16}$$

where $\beta = 0.4$ [12]. Additionally, the stress concentration can be defined by

$$\begin{aligned} k_{22}(\varphi) = {} & \frac{V_f E_2^f + (1-V_f)[\beta E_2^f + (1-\beta)E^m]}{\beta E_2^f + (1-\beta)E^m}\left\{1 + \frac{a}{2}\sqrt{V_f}\cos(2\varphi)\right. \\ & + \frac{b}{2(1-\sqrt{V_f})}[V_f^2\cos(4\varphi) + 4(1 - 2\cos(2\varphi))V_f\cos^2(\varphi)] \\ & \left. + \sqrt{V_f}(2\cos(2\varphi) + \cos(4\varphi))\right\} \end{aligned} \tag{17}$$

$$k_{22}^c = k_{22}(\phi) \tag{18}$$

$$k_{22}^t = k_{22}(0) \tag{19}$$

where

$$\phi = \frac{\pi}{4} + \frac{1}{2}\operatorname{asin}\left(\frac{S_c^m - S_t^m}{S_c^m + S_t^m}\right) \tag{20}$$

$$a = \frac{[1 - \nu^m - 2(\nu^m)^2]E_2^f - [1 - \nu_{23}^f - 2(\nu_{23}^f)^2]E^m}{(1+\nu^m)E_2^f + [1 - \nu_{23}^f - 2(\nu_{23}^f)^2]E^m} \tag{21}$$

$$b = \frac{(1+\nu_{23}^f)E^m - (1+\nu^m)E_2^f}{[\nu^m + 4(\nu^m)^2 - 3]E_2^f - (1+\nu_{23}^f)E^m} \tag{22}$$

3. A novel elasticity-based modeling approach

This Section presents a novel elasticity-based model to obtain analytical closed-form expressions for transversal strengths. Some recent advances from the literature are employed as a guide, considering two main failure mechanisms: matrix cavitation for tension [7,26] and fiber–matrix interface debonding for compression [5,29]. The use of these failure mechanisms requires stress distributions to properly estimate the strength. First, an analytical solution for stress distribution in a single inclusion is presented [19]. Afterwards, in order to expand this solution for laminae with a real range of fiber volume fraction, the finite element simulations are carried out to define the adjustment functions. Finally, once the closed expression is derived, the average values of critical dilatational energy is employed to estimate transverse tensile strength while the interface strength is employed to estimate the compressive strengths. The obtained theoretical results are compared with the available experimental data, see Tables 1–3 for details.

3.1. Stress distribution and finite element analysis

Stress distribution on the fiber–matrix interface is estimated using the solution [19] for the stress around a circular elastic inclusion perfectly bonded in an infinite elastic medium under plane strain condi-

Table 1
References used for transversal tensile strength experimental data.

References	Fiber
Aboudi [34]	carbon
Falcó *et al.* [35]	carbon
Gopalakrishnan *et al.* [36]	glass
Hsiao & Daniel [37]	carbon
Kaddour & Hinton [38]	carbon and glass
Kaddour *et al.* [39]	glass
Kaddour *et al.* [40]	carbon and glass
Namdar & Darendeliler [41]	carbon
Soden *et al.* [42]	carbon and glass
Perogamvros & Lampeas [43]	carbon
Reddy *et al.* [44]	glass

Table 2
References used for transversal compressive strength experimental data.

References	Fiber
Falcó *et al.* [35]	carbon
Kaddour & Hinton [38]	carbon and glass
Kaddour *et al.* [40]	carbon and glass
Lee & Soutis [45]	carbon
Namdar & Darendeliler [41]	carbon
Perogamvros & Lampeas [43]	carbon
Soden *et al.* [42]	carbon and glass

Table 3
References used for transversal shear strength experimental data.

References	Fiber
Kaddour & Hinton [38]	carbon and glass
Kaddour *et al.* [40]	carbon and glass

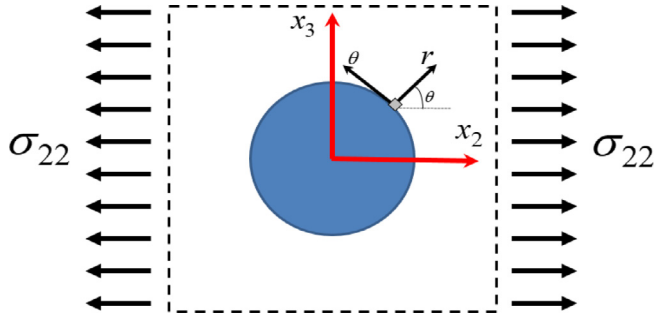

Fig. 3. Coordinate system to compute the stress distribution in a fiber embedded in infinite matrix.

tion. Fig. 3 shows an idealized arrangement of fiber embedded in matrix and the coordinate system to compute the stress distribution. Note that this representation does not consider any interaction between neighboring fibers; in other words, it assumes $V_f \to 0$. Considering a uniaxial transversal load in a region far from the fiber, the non-zero stress components on the interface are

$$\sigma_{rr}^{m}(\sigma_{22},\theta) = \frac{\sigma_{22}}{2}[(1-\gamma)+(1-\beta)\cos(2\theta)] \tag{23}$$

$$\sigma_{\theta\theta}^{m}(\sigma_{22},\theta) = \frac{\sigma_{22}}{2}[(1+\gamma)-(1+3\beta)\cos(2\theta)] \tag{24}$$

$$\sigma_{r\theta}^{m}(\sigma_{22},\theta) = -\frac{\sigma_{22}}{2}[(1-\beta)\sin(2\theta)] \tag{25}$$

$$\sigma_{zz}^{m}(\sigma_{22},\theta) = \nu^{m}[\sigma_{rr}^{m}(\sigma_{22},\theta)+\sigma_{\theta\theta}^{m}(\sigma_{22},\theta)] \tag{26}$$

where

$$\kappa^{f} = 3-4\nu_{23}^{f} \tag{27}$$

$$\kappa^{m} = 3-4\nu^{m} \tag{28}$$

$$\alpha = \frac{G^{m}\kappa^{f}-G_{23}^{f}\kappa^{m}}{G_{23}^{f}+G^{m}\kappa^{f}} \tag{29}$$

$$\beta = \frac{G^{m}-G_{23}^{f}}{G^{m}+G_{23}^{f}\kappa^{m}} \tag{30}$$

$$\gamma = \frac{\alpha-\beta}{(1-\beta)-\beta(1-\alpha)} \tag{31}$$

where ν^{m} is the matrix Poisson's ratio, ν_{23}^{f} is the fiber transversal Poisson's ratio, G^{m} is the matrix shear modulus and G_{23}^{f} is the fiber transversal shear modulus.

The solution proposed by Honein & Herrman [19] evaluated the stress distribution for isotropic materials, that can be also applied for transversally isotropic material if the isotropic plane coincides with the transversal inclusion plane, such as carbon fibers [20]. Finite element method is employed to evaluate the stress distribution for a finite medium ($V_f \neq 0$), defining adjustment functions. The general finite element procedure is introduced in the sequence.

The first step is to compute the effective elastic properties of unidirectional lamina considering a procedure based on [21,22]. The RVE is presented in Fig. 4 assuming that fiber distribution has a square pattern. Capital letters are used to denote six faces, while the lower index coincides with the coordinate system and the top index indicates the orientation. Each edge length is L_i in the direction x_i. The displacement between two parallel faces must be constant along all the faces due to symmetry. Mathematically, this condition is defined by

$$u_i^{(J+)} - u_i^{(J-)} = \lambda_i^{(J)} \tag{32}$$

where $\lambda_i^{(J)}$ is the constant displacement between faces $J+$ and $J-$ on the direction i, $u_i^{(J+)}$ and $u_i^{(J-)}$, respectively.

The computation of the effective elastic properties has three steps allowing estimation of all five independent properties, see Fig. 5a. This is done by considering a displacement driven condition, and the reaction forces are computed from the equilibrium conditions. Strains are

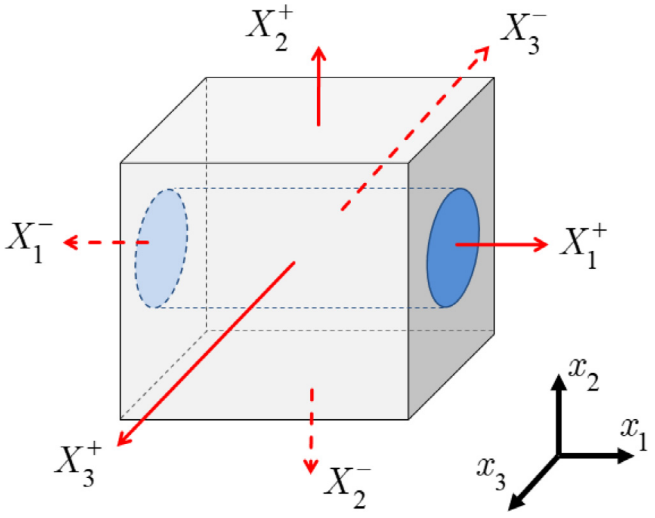

Fig. 4. RVE indicating the faces where the displacements are imposed to define symmetrical conditions.

computed from the displacements using geometrical definitions while stresses are evaluated from the forces. Stress distribution is not uniformly distributed in the RVE, but the homogenization procedure uses this hypothesis to compute effective properties.

The first step is to compute c_{1111} and c_{1122}. A uniformly distributed displacement δ_{11} is applied at face X_1^+ in the direction x_1, denoted by $u_1^{(1+)} = \delta_{11}$. The boundary conditions are defined by $u_1^{(1-)} = u_2^{(2+)} = u_2^{(2-)} = u_3^{(3+)} = u_3^{(3-)} = 0$. The normal strain in x_1 direction is computed by $\langle \varepsilon_{11} \rangle = \delta_{11}/L_1$. Using the reactions forces from the finite element solution on face X_1^+ in x_1 direction, F_{11}, and on face X_2^+ in x_2 direction, F_{22}, the normal stress components are computed by $\langle \sigma_{11} \rangle = F_{11}/L_2L_3$ and $\langle \sigma_{22} \rangle = F_{22}/L_1L_3$. Finally, the effective properties are computed by $c_{1111} = \langle \sigma_{22} \rangle / \langle \varepsilon_{11} \rangle$ and $c_{1122} = \langle \sigma_{22} \rangle / \langle \varepsilon_{11} \rangle$.

Similar steps are carried out for the other effective elastic properties. The estimation of c_{2222} and c_{2233}, considers the displacement $u_2^{(2+)} = \delta_{22}$ and the boundary conditions $u_1^{(1+)} = u_1^{(1-)} = u_2^{(2-)} = u_3^{(3+)} = u_3^{(3-)} = 0$. The transversal strain is given by $\langle \varepsilon_{22} \rangle = \delta_{22}/L_2$, and stresses are $\langle \sigma_{22} \rangle = F_{22}/L_1L_3$ and $\langle \sigma_{33} \rangle = F_{33}/L_1L_2$. Therefore, the effective properties are $c_{2222} = \langle \sigma_{22} \rangle / \langle \varepsilon_{22} \rangle$ and $c_{2233} = \langle \sigma_{33} \rangle / \langle \varepsilon_{22} \rangle$.

The third and last step evaluates elastic property c_{1212} by assuming the displacement $u_1^{(2+)} = \delta_{21}$ and the boundary conditions $u_2^{(1+)} = u_2^{(1-)} = u_3^{(1+)} = u_3^{(1-)} = u_1^{(2-)} = u_2^{(2+)} = u_2^{(2-)} = u_3^{(2+)} = u_3^{(2-)} = u_2^{(3+)} = u_2^{(3-)} = u_3^{(3+)} = u_3^{(3-)} = 0$. The in-plane shear strain and stress are computed by $\langle \varepsilon_{12} \rangle = \delta_{21}/2L_2$ and $\langle \sigma_{12} \rangle = F_{21}/L_1L_3$, which results in the effective property $c_{1212} = \langle \sigma_{12} \rangle / 2\langle \varepsilon_{12} \rangle$.

Once all the independent components of the elasticity tensor are computed, the effective engineering constants of the lamina are computed using the following relations:

$$E_1 = \frac{c_{1111}(c_{2222} + c_{2233}) - 2c_{1122}^2}{c_{2222} + c_{2233}} \tag{33}$$

$$E_2 = \frac{c_{1111}(c_{2222}^2 - c_{2233}^2) - 2c_{1122}^2(c_{2222} - c_{2233})}{c_{1111}c_{2222} - c_{1122}^2} \tag{34}$$

$$\nu_{12} = -\frac{c_{1122}}{c_{2222} + c_{2233}} \tag{35}$$

$$G_{12} = c_{1212} \tag{36}$$

$$G_{23} = \frac{c_{2222} - c_{2233}}{2} \tag{37}$$

Finite element package ANSYS is applied for the calculations using a higher order element SOLID 186. After a convergence analysis, a mesh with two elements through direction x_1; between 80 and 120 elements along the fiber diameter perimeter, depending of V_f; and between 7 and 10 along the fiber in radial direction from as inner square created just to improve the mesh generation. Fig. 5b shows a mesh employed for $V_f = 0.6$ and the boundary conditions. The contact between fiber and matrix is assumed as perfectly bonded, with no separation or slippage, with the formulation MPC (Multi Point Constraints). This type of contact improves the model computational performance [23].

The adjustment function is defined after the determination of elastic properties. This is done by considering uniaxial transversal load treated in the sequence: transversal tensile strength and transversal compressive strength.

3.2. Transversal tensile strength

According to Elnekhaily & Talreja [7], damage onset in unidirectional laminae subjected to tensile transversal load is characterized by matrix cavitation around the fiber with $\theta = 0^\circ$ with the dilatational energy density as the driving effect, since it is under triaxial stress state on the matrix. The dilatational energy density is computed by

$$u_v = \left(\frac{1 - 2\nu^m}{6E^m}\right)(\sigma_{ii}^m)^2 \tag{38}$$

The critical point for cavitation occurs for $\theta = 0^\circ$, which has the following stress components according to the stress distribution presented in the previous Section:

$$\sigma_{rr}^m(\sigma_{22}, 0) = \frac{\sigma_{22}}{2}[(1 - \gamma) + (1 - \beta)] \tag{39}$$

$$\sigma_{\theta\theta}^m(\sigma_{22}, 0) = \frac{\sigma_{22}}{2}[(1 + \gamma) - (1 + 3\beta)] \tag{40}$$

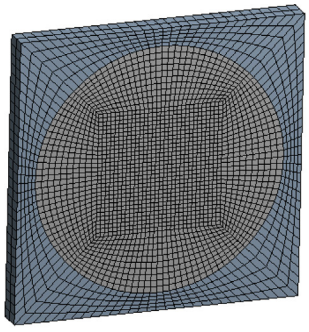

(a)

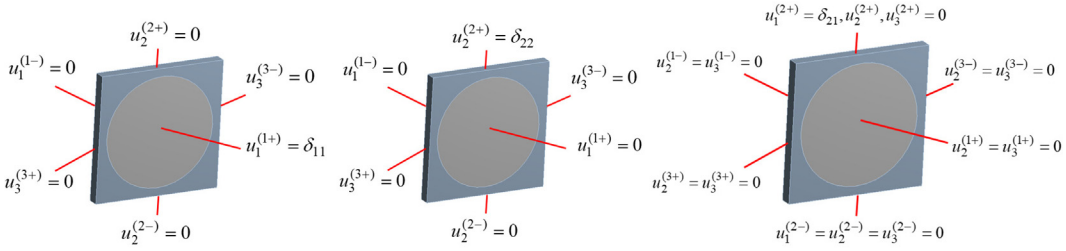

(b)

Fig. 5. Finite element model for the representative volume element. (a) Meshed RVE for $V_f = 0.6$; (b) boundary conditions.

$$\sigma^m_{r\theta}(\sigma_{22},0)=0 \tag{41}$$

$$\sigma^m_{zz}(\sigma_{22},0)=\nu^m[\sigma^m_{rr}(\sigma_{22},0)+\sigma^m_{\theta\theta}(\sigma_{22},0)]=\nu^m\sigma_{22}(1-2\beta) \tag{42}$$

Substituting Eqs. (39)–(42) into Eq. (38),

$$u_v(V_f\to 0)=\left(\frac{1-2\nu^m}{6E^m}\right)[(1+\nu^m)(\sigma_{22})(1-2\beta)]^2 \tag{43}$$

Eq. (43) is the dilatational energy density for a single fiber embedded in an infinite matrix. In order to represent a general case for any fiber volume fraction, an adjustment function $g_t(V_f)$ is introduced to relate the stress σ^m_{ii} for $V_f\to 0$ with the stress components σ^m_{ii} for actual values of V_f. In other words, $u_v(V_f)=u_v(V_f\to 0)g_t(V_f)$. Hence, Eq. (43) can be adapted for $V_f\neq 0$ using the following expression:

$$u_v=\left(\frac{1-2\nu^m}{6E^m}\right)[(1+\nu^m)(\sigma_{22})(1-2\beta)g_t(V_f)]^2 \tag{44}$$

The definition of the adjustment function $g_t(V_f)$ is carried out with finite element simulations, considering a uniaxial load applied on the RVE where the unique non-zero stress component is $\langle\sigma_{22}\rangle$. As previously presented, a uniform displacement must be applied on the faces of the RVE. For simplicity, fixing $u_1^{(1-)}=u_2^{(2-)}=u_3^{(3-)}=0$, the normal strains are computed by $\langle\varepsilon_{11}\rangle=\delta_{11}/L_1$, $\langle\varepsilon_{22}\rangle=\delta_{22}/L_2$ and $\langle\varepsilon_{33}\rangle=\delta_{33}/L_3$, where $u_1^{(1+)}=\delta_{11}$, $u_2^{(2+)}=\delta_{22}$ and $u_3^{(3+)}=\delta_{33}$. Using these definitions, considering normal stresses and strains, displacement applied on the positive faces are $u_1^{(1+)}=\delta_{11}=(-\nu_{12}/E_1)L_1\langle\sigma_{22}\rangle$, $u_2^{(2+)}=\delta_{22}=(1/E_2)L_2\langle\sigma_{22}\rangle$ and $u_3^{(3+)}=\delta_{33}=(-\nu_{12}/E_1)L_3\langle\sigma_{22}\rangle$.

A set of finite element numerical simulations is carried out applying this displacement field with $0.3\leqslant V_f\leqslant 0.7$ for CFRP and GFRP in order to define the adjustment function. The maximum value σ^m_{ii} on the interface is obtained, and results, normalized by the applied load σ_{22}, $\max(\sigma^m_{ii})/\sigma_{22}$, are shown in Fig. 6, where the triangles and circles are the FE results and the lines are the calibrated adjustment functions. The numerical calibration employs the Levenberg-Marquardt algorithm [24] and the following expression is obtained:

$$g_t(V_f)=1-5.8\gamma V_f^3 \tag{45}$$

The idea to use finite element solutions to obtain expressions for stress and strain distributions is also presented in [25], but using Fourier series. Nevertheless, closed expressions are not presented. The main advantage of the novel proposed approach is that only the $\max(\sigma^m_{ii})/\sigma_{22}$ should be obtained instead of the whole distribution, resulting in a simple equation.

Damage onset due to the matrix cavitation is defined by $u_v=u_v^c$ [7]. Lamina rupture does not coincide exactly with the damage onset, which means that there is a difference between the damage onset and rupture due to damage propagation. For the sake of simplicity, this study assumes a perfectly brittle matrix behavior. Despite that some matrix materials are not perfectly brittle, the usual experimental stress–strain curves for unidirectional laminae subjected to transversal loads is almost linear up to rupture, see [38,40,42], indicating a brittle behavior, mainly for transverse tensile load. Mathematically, that means that $u_v=u_v^c$ coincides with $\sigma_{22}=S^t_{22}$. Hence, manipulating Eq. (44), transversal tensile strength of lamina is estimated by

$$S^t_{22}=\frac{1}{(1+\nu^m)(1-2\beta)(1-5.8\gamma V_f^3)}\sqrt{\left(\frac{6E^m}{1-2\nu^m}\right)u_v^c} \tag{46}$$

The main difficulty for the use of Eq. (46) is that u_v^c must be measured in a triaxial tensile test [26]. Two different approaches are suggested here, and a further verification is discussed in the Section 4. The first one considers a set of experimental data, defining an average value of u_v^c for epoxy matrices. Alternatively, u_v^c is assumed proportional to S^m_t, $u_v^c=\xi S^m_t$, where ξ is calibrated according to experimental data. The first approach uses Eq. (46), while the second is using the following equation:

$$S^t_{22}=\frac{\xi}{(1+\nu^m)(1-2\beta)(1-5.8\gamma V_f^3)}S^m_t \tag{47}$$

Note that $\xi=1$ is equivalent to uniaxial tensile test. According to Elnekhaily & Talreja [26], 0.13 MPa $< u_v^c <$ 0.20 MPa. Eq. (46) also allows an application of inverse problem: u_v^c can be obtained for any matrix with one experimental measured value of S^t_{22}.

3.3. Transversal compressive strength

The compressive load is assumed to have a failure driven by the interface. Therefore, the following failure function [5] can be employed to establish the transversal compressive strength:

$$f_i=\left(\frac{\max(0,t_{rr})}{S^i_n}\right)^2+\left(\frac{t_{r\theta}}{S^i_s}\right)^2+\left(\frac{t_{rz}}{S^i_s}\right)^2 \tag{48}$$

where t_{rr}, $t_{r\theta}$ and t_{rz} are the interface tractions and S^i_n and S^i_s are the normal and shear interface strengths, respectively. Interface failure is defined by $f_i=1$. For the sake of simplicity, normal and shear strengths are assumed to have the same values, i.e., $S^i_s=S^i_n=S^i$. It is difficult to

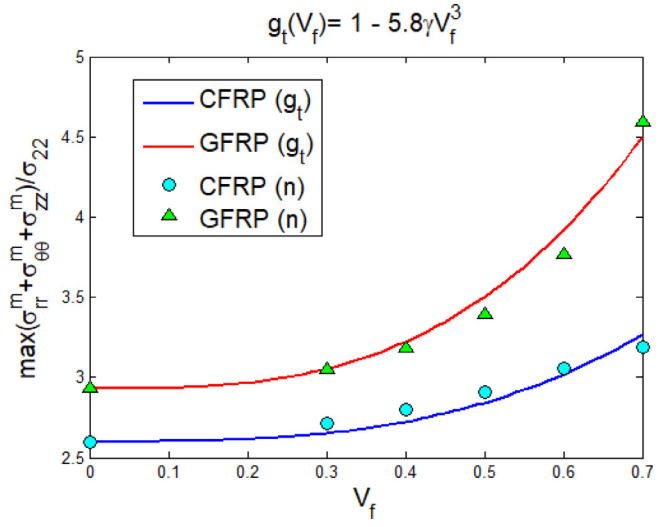

Fig. 6. Numerical calibration of the transversal tensile strength model for $V_f\neq 0$.

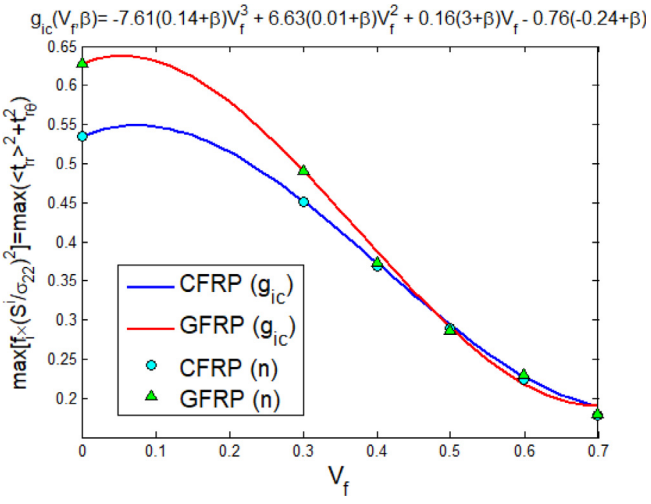

Fig. 7. Numerical calibration of the transversal compressive strength model for $V_f\neq 0$.

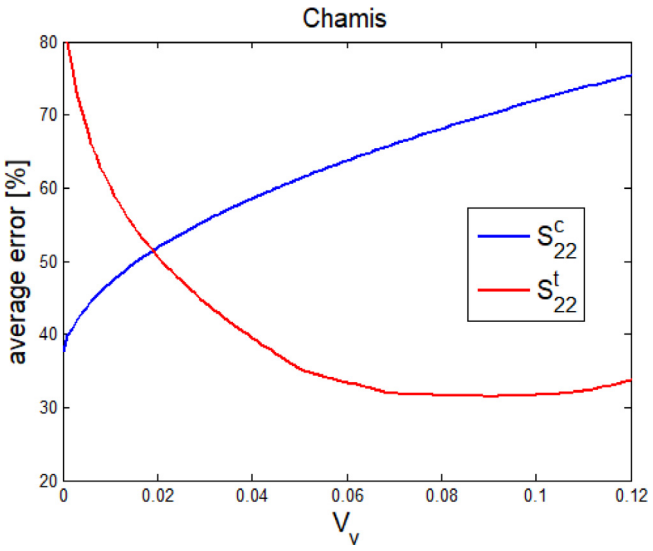

Fig. 8. Calibration of the void volume fraction, V_v, of the Chamis model.

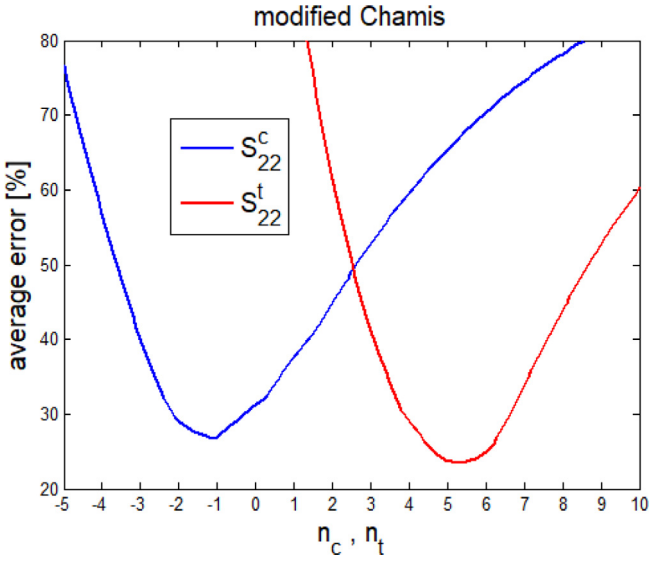

Fig. 9. Calibration of the exponents of the modified Chamis model.

measure the interface strength. Assumption of $S_s^i = S_n^i = S^i$ and other simplification are also adopted in [27–29].

Using the stress distribution discussed in the previous section, the failure condition for $V_f \to 0$ is

$$f_i^{\max}(V_f \to 0) = \left(\frac{\sigma_{22}}{S^i}\right)^2 \left(\frac{1-\beta}{2}\right)^2 = 1 \tag{49}$$

In order to generalize this criterion, an adjustment function $g_{ic}(V_f)$ is employed, defining the failure criterion as follows:

$$f_i^{\max}(V_f) = f_i^{\max}(V_f \to 0) g_{ic}(V_f) = \left(\frac{\sigma_{22}}{S^i}\right)^2 \left(\frac{1-\beta}{2}\right)^2 g_{ic}(V_f) \tag{50}$$

A similar calibration procedure is carried out in order to define the adjustment function, $g_{ic}(V_f)$, using results of finite element simulations (see Fig. 7) and the following expression is obtained:

$$g_{ic}(V_f) = -7.71(0.14+\beta)V_f^3 + 6.63(0.01+\beta)V_f^2 + 0.16(3+\beta)V_f - 0.76(-0.24+\beta) \tag{51}$$

Under these assumptions, the failure occurs with $\sigma_{22} = -S_{22}^c$ and $f_i^{\max}(V_f) = 1$, which defines the transversal compressive strength of lamina as follows

$$S_{22}^c = \frac{S^i}{\sqrt{g_{ic}(V_f)}} \left(\frac{2}{1-\beta}\right) \tag{52}$$

3.4. Transversal shear strength

Transversal shear strength can be defined by different ways. Fenner & Daniel [30] suggested that it is equal to the transversal tensile strength, $S_{23}^s = S_{22}^t$. Dávila *et al.* [31] suggested use of the Mohr-Coulomb failure criterion in order to associate transversal shear strength with the transversal compressive strength. A generalization of both ideas can be defined with the following equations:

$$S_{23}^s = \alpha_t S_{22}^t \tag{53}$$

$$S_{23}^s = \alpha_c S_{22}^c \tag{54}$$

where α_t and α_c are constants.

Alternatively, the transversal shear strength is estimated using only the matrix shear strength by the following equation:

$$S_{23}^s = \alpha_s S_s^m \tag{55}$$

where α_s is a constant to be calibrated.

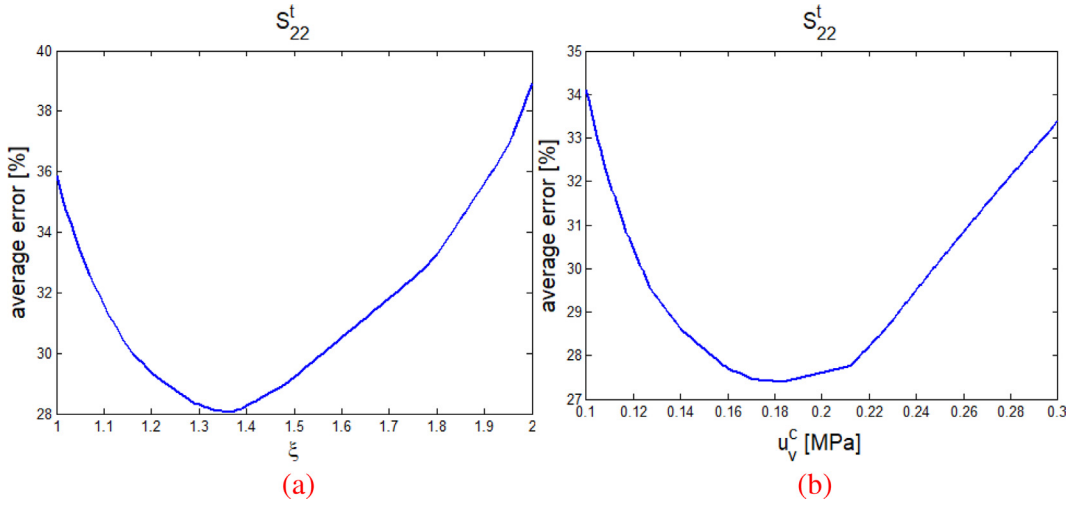

Fig. 10. Calibration of the novel elasticity-based model for transversal tensile strength: (a) assuming $u_v^c = \xi S_t^m$; (b) assuming an average value of u_v^c.

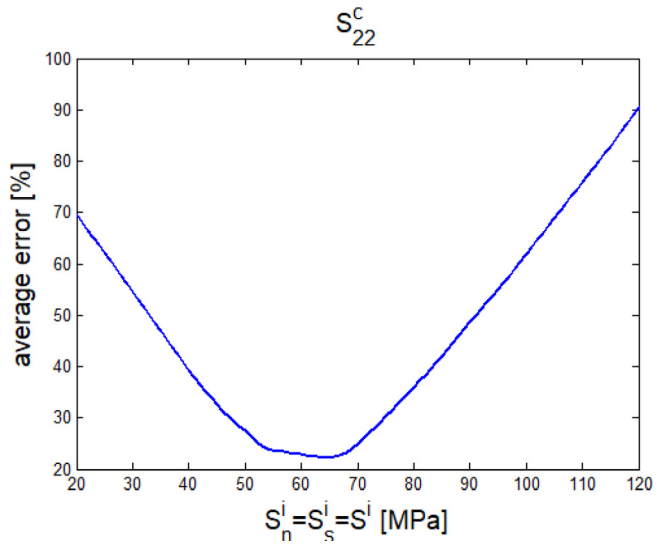

Fig. 11. Calibration of the average interfacial strength for the novel elasticity-based model for transversal compressive strength.

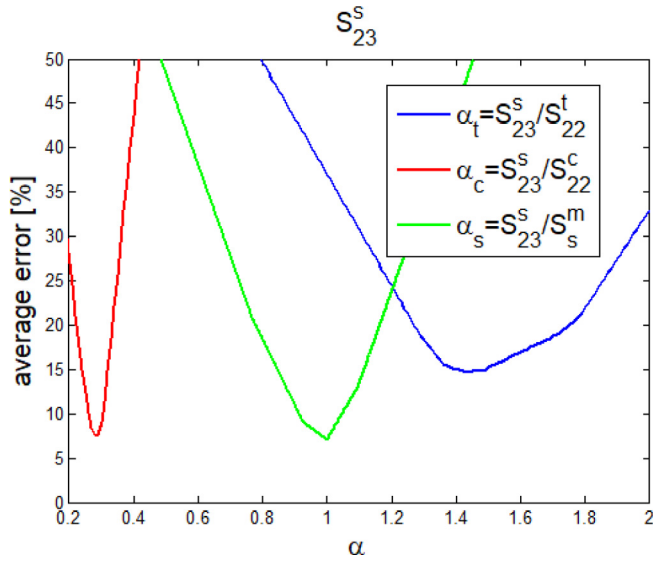

Fig. 12. Calibration of the proportionality constants α of the novel elasticity-based model for transversal shear strength.

4. Results

This Section applies different micromechanical models to obtain the macroscopic transversal strength of unidirectional laminae. The models discussed in the preceding sections are employed for this purpose and compared with experimental data. In this regard, it should be noted that the experimental data for the composite materials commonly have high uncertainty due to irregular arrangement of fibers. For example, the fabrication and cure process can induce significant fiber misalignment, voids, residual stresses and shape distortion [32]. An extensive discussion about the modeling of manufacturing process of the composite materials is given in [33].

The experimental data employed as reference consider a set of experiments compiled from the literature: 31 data for S^t_{22}, 18 data for S^c_{22} and 9 data for S^s_{23}. The references for these data and the types of fibers are given in Tables 1–3. A calibration of the following parameters must be carried out: void volume fraction for the Chamis model; exponents of the modified Chamis model; critical dilatational energy, interface strength, and proportionality constants for transverse tensile, compressive and shear strengths for the proposed models. These parameters are not usual input based on WWFE guidelines that employ only the constituents' properties. The calibration is based on the analysis of the average error, being estimated by the sum of the absolute error of each estimation divided by the amount of experimental data. The idea is to choose parameters that minimize the error. It should be highlighted that the goal is to obtain an estimation of average values of these parameters assuming that just the constituents' properties as input.

Initially, the classical Chamis model is employed to evaluate tensile and compressive transversal strengths. The influence of the volume fraction of voids, V_v, is presented in Fig. 8. Results indicate that $V_v = 0.09$ leads to the minimum error for tensile load, while $V_v = 0$ leads to the best prediction in compression. Note that $V_v = 0.09$ is considerably higher than the actual values for the laminae. The differences between both curves point to inconsistent results due to semi-empirical nature of this model.

The modification of the Chamis model, proposed in Section 3, provides a considerable improvement when compared with the classical Chamis model. Fig. 9 presents results of the error analysis indicating that the parameters $n_t = 5$ and $n_c = -1$ have result in a minimum analysis.

The novel elasticity-based model is now addressed and Fig. 10 indicates that both approaches for tensile strength, assuming $u^c_v \propto \xi$ or obtaining an average value for u^c_v, have close estimations, with an average error around 28%. By using the minimum value of both curves, it is obtained $\xi = 1.35$ and $u^c_v = 0.18$ MPa.

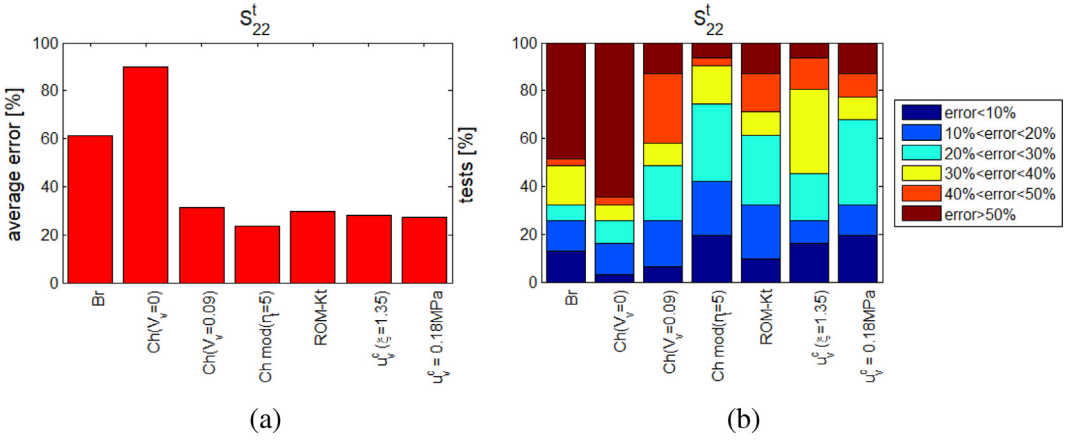

Fig. 13. Results for the transversal tensile strength S^t_{22}:(a) average error; (b) ranges of errors.

The analysis of transversal shear strength presented in Fig. 11 shows the value of $S^i = 65$MPa obtained for the best estimation, which is the one associated with an average error of 22%, the minimum value of the curve. This value is in agreement with many reports in the literature: Totry *et al.* [27] employed 57.55 MPa, Tang *et al.* [28] suggested 69 MPa for usual interfaces and Varandas *et al.* [46] and Chevalier *et al.* [47] used 50 MPa for normal strength and 75 MPa for shear strength.

Finally, the analysis of transversal shear strength is evaluated in Fig. 12 showing the influence of the proportionality constants assumed in Section 3. The minimum error points are associated with the following values:$\alpha_t = 1.43$, $\alpha_c = 0.28$ and $\alpha_s = 1$.

After the calibration, the strength properties of the different approaches are compared. The procedure proposed in Vignoli *et al.* [2] is applied to calculate the absolute values of the average errors and the ranges of errors are evaluated. Fig. 13 shows the average error and the error ranges for transversal tensile strength, S^t_{22}, considering a set of 31 experimental data compiled from the references listed in the Table 1. The average error represents the easiest comparison but, due to high dispersion of experimental data, one critical value may distort the conclusion. The range of errors is calculated by considering the absolute error of each estimation, classifying the error prediction smaller than 10%, between 10% and 20%, between 20% and 30%, between 30% and 40%, between 40% and 50% and higher than 50%. Therefore, average errors and ranges of errors are helpful for uncertainty quantification process, indicating in a quantitative way the most probable error from each prediction. Note that the closest predictions are obtained using the proposed model with $u^c_v = 0.18$ MPa, while the traditional Chamis model with $V_v = 0$ leads to the worst one.

Based on these results, the following conclusions are made:

(i) Bridging and Chamis models with $V_v = 0$ lead to the average error higher than the simple ROM modified to include stress concentration effect (ROM-Kt);
(ii) Chamis model with $V_v = 0.09$ presents the average error of 31.5%, while for $V_v = 0$ it is 90.1%, but $V_v = 0.09$ is not representative of real laminae;
(iii) by comparing both approaches based on the dilatational energy density, assuming $u^c_v = \xi S^m_t$ with $\xi = 1.35$ the average error is 28.1% while considering an average value $u^c_v = 0.18$ MPa the average error is 27.4%;
(iv) despite the difficulty to measure u^c_v, $u^c_v = 0.18$ MPa is recommended as an average value suitable for epoxy matrix;
(v) the proposed modified Chamis model and the elasticity-based model using $u^c_v = 0.18$ MPa lead to the smallest average errors: 23.8% and 27.4%, and the highest amount of cases with errors smaller than 30%, 74.2% and 67.7%.

The analysis of transversal compressive strength, S^c_{22} is performed considering a set of 18 experimental data compiled from the references listed in the Table 2. Fig. 14 shows the average error and the error ranges. The closest predictions are obtained using the proposed model

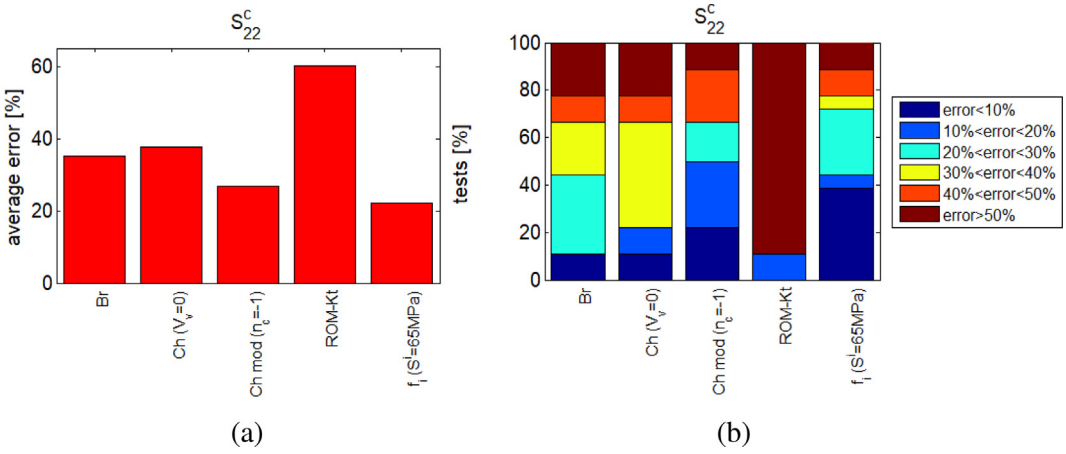

Fig. 14. Results for the transversal compressive strength S^c_{22}: (a) average error; (b) ranges of errors.

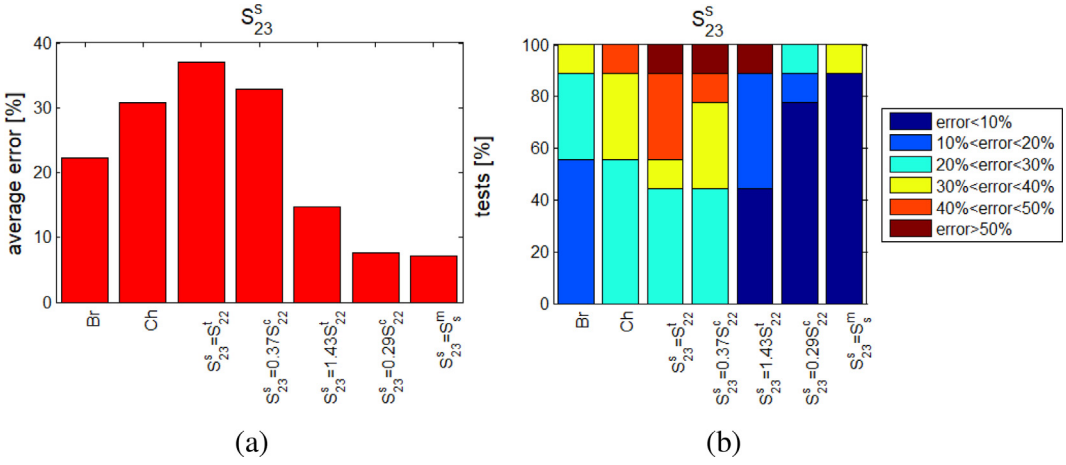

Fig. 15. Results for the transversal shear strength S^s_{23}: (a) average error; (b) ranges of errors.

for interface failure, while ROM-Kt leads to the worst one. Based on these results the following conclusions are made:

(i) Bridging and Chamis models lead to the average errors higher than 35%;
(ii) for ROM-Kt, the average error increases considerable for compressive strength comparing with the tensile strength;
(iii) the modified Chamis model leads to an average error of 26.9%, and 66.7% of the cases lead to an error smaller than 30%;
(iv) the proposed elasticity-based model that assumes interface failure with $S^i = 65$ MPa leads to an average error of 22.1%, and 38.9% of the cases lead to an error smaller than 30%;
(v) the proposed elasticity-based models for S^t_{22} and S^c_{22} do not require the matrix strengths as input, and the average values $u^c_v = 0.18$ MPa and $S^i = 65$ MPa can be set with the reasonable estimations.

The analysis of the transversal shear strength, S^s_{23}, is performed considering a set of 9 experimental data compiled from the references listed in the Table 3. Fig. 15 shows the average error and the error ranges. It is observed that the closest predictions are obtained estimating transversal shear strength equal to matrix strength, while the estimation of transversal shear strength equal to transversal tensile strength leads to the worst prediction. Based on these results, the following conclusions are made:

(i) Bridging and Chamis models lead to the better predictions for S^s_{23} than for other transversal strengths, with average errors equal to 22.3% and 30.8%, respectively;
(ii) the estimation of $S^s_{23} = S^t_{22}$, as suggested by Fenner & Daniel [30], results in an average error equal to 37%, while the generalized approach $S^s_{23} = \alpha_t S^t_{22}$, with $\alpha_t = 1.43$ and S^t_{22} computed using Eq. (46), leads to an average error equal to 14.7%;
(iii) the estimation of $S^s_{23} = 0.37 S^c_{22}$, as suggested by Dávila *et al.* [31], results in an average error equal to 31.4%, while the generalized approach $S^s_{23} = \alpha_c S^c_{22}$, with $\alpha_c = 0.29$ and S^c_{22} computed using Eq. (52), leads to an average error equal to 7.6%;
(iv) the estimation of $S^s_{23} = S^m_s$ is the simplest approach and it leads to the best prediction with average error equal to 7%;
(v) by considering the error range evaluation, estimations $S^s_{23} = 0.29 S^c_{22}$ and $S^s_{23} = S^m_s$ lead to the errors smaller than 10% for 77.8% and 88.9% of the cases, respectively.

5. Conclusions

A novel micromechanical analysis approach based on transversal tension, compression and shear strengths is proposed to deal with the composite material design. An overview of analytical models is presented for unidirectional laminae. The first approach is based on the Chamis model adding a calibrated parameter according to the experimental data. The second one uses an elastic solution together with a calibration approach based on finite element simulations. The estimation of the tensile strengths is based on the dilatational energy density while the estimation of the compressive strength is based on the interface strength. The transversal shear strength of lamina is estimated on the basis of the matrix shear strength. A set of 58 experimental data is compiled and compared with predictions of the analytical models, including 31 experimental data for transversal tensile strength S^t_{22}, 18 experimental data for transversal compressive strength S^c_{22} and 9 experimental data for transversal shear strength S^s_{23}. It is shown that the newly proposed models lead to considerable improvements in the estimation of the transversal strength in comparison with the previously formulated analytical models.

Declaration of Competing Interest

The authors declare that they have no known competing financial interests or personal relationships that could have appeared to influence the work reported in this paper.

Acknowledgements

The authors acknowledge support of the Brazilian Research Agencies CNPq, CAPES, FAPERJ, and the Natural Sciences and Engineering Research Council of Canada (NSERC).

References

[1] Hinton MJ, Kaddour AS, Soden PD. Failure Criteria in Fibre Reinforced Polymer Composites: The World-Wide Failure Exercise. Elsevier; 2004.
[2] Vignoli LL, Savi MA, Pacheco PMCL, Kalamkarov AL. Comparative analysis of micromechanical models for the elastic composite laminae. Composites Part B - Eng 2019;174:106961.
[3] Huang ZM. On micromechanics approach to stiffness and strength of unidirectional composites. J Reinf Plast Compos 2019;38:167–96.
[4] Herráez M, González C, Lopes CS, Guzmán de Villoria R, Llorca J, Varela T, et al. Computational micromechanics evaluation of the effect of fibre shape on the transverse strength of unidirectional composites: An approach to virtual materials design. Compos A Appl Sci Manuf 2016;91:484–92.
[5] Macedo RQ, Ferreira RTL, Guedes JM, Donadon MV. Intraply failure criterion for unidirectional fiber reinforced composites by means of asymptotic homogenization. Compos Struct 2017;159:335–49.
[6] Wongsto A, Li S. Micromechanical FE analysis of UD fibre-reinforced composites with fibres distributed at random over the transverse cross-section. Compos A 2005;36:1246–66.
[7] Elnekhaily SA, Talreja R. Damage initiation in unidirectional fiber composites with different degrees of nonuniform fiber distribution. Compos Sci Technol 2018;155:22–32.
[8] Andrianov IV, Awrejcewicz J, Danishevs'kyy VV. Asymptotical Mechanics of Composites – Modelling Composites without FEM. Springer; 2018.
[9] Tsai SW, Melo JDD. An invariant-based theory of composites. Compos Sci Technol 2014;100:237–43.
[10] Daniel IM, Ishai O. Engineering mechanics of composite materials. 2nd ed.,. Oxford University Press; 2006.
[11] Chamis CC, Abdi F, Garg M, Minnetyan L, Baid H, Huang D, et al. Micromechanics-based progressive failure analysis prediction for WWFE-III composite coupon test cases. J Compos Mater 2013;47:2695–712.
[12] Huang ZM, Liu L. Predicting strength of fibrous laminates under triaxial loads only upon independently measured constituent properties. Int J Mech Sci 2014;79:105–29.
[13] Catalanotti G. Prediction of in situ strengths in composites: Some considerations. Compos Struct 2019;207:889–93.
[14] Soden PD, Kaddour AS, Hinton MJ. Recommendations for designers and researchers resulting from the world-wide failure exercise. Compos Sci Technol 2004;64:589–604.
[15] Kaddour AS, Hinton MJ. Maturity of 3D failure criteria for fibre reinforced composites: Comparison between theories and experiments: Part B of WWFE-II. J Compos Mater 2013;47:925–66.
[16] Gibson RF. Principle of composite material mechanics. McGraw-Hill; 1994.
[17] Agarwal BD, Broutman LJ, Chandrashekhara K. Analysis and performance of fiber composites. 3rd ed. Wiley; 2006.
[18] Devireddy SBR, Biswas S. Effect of fiber geometry and representative volume element on elastic and thermal properties of unidirectional fiber-reinforced composites. J Compos 2014:629175.
[19] Honein T, Herrmann G. On bonded inclusions with circular or straight boundaries in plane elastostatics. J Appl Mech 1990;57:850–6.
[20] Mantic V. Interface crack onset at a circular cylindrical inclusion under a remote transverse tension. Application of a coupled stress and energy criterion. Int J Solids Struct 2009;46:1287–304.
[21] Barbero EJ. Finite element analysis of composite materials. CRC Press; 2008.
[22] Tita V, Medeiros R, Marques FD, Moreno ME. Effective properties evaluation for smart composite materials with imperfect fiber-matrix adhesion. J Compos Mater 2015;49:3683–701.
[23] Lee HH. Finite element simulations with ANSYS workbench 14. SDC Publications; 2014.
[24] Nocedal J, Wright SJ. Numerical optimization. Springer; 1999.
[25] Oh JH, Jin KK, Ha SK. Interfacial strain distribution of a unidirectional composite with randomly distributed fibers under transverse loading. J Compos Mater 2006;40:759–78.
[26] Elnekhaily SA, Talreja R. Effect of axial shear and transverse tension on early failure events in unidirectional polymer matrix composites. Compos A 2019;119:275–82.
[27] Totry E, González C, Llorca J. Failure locus of fiber-reinforced composites under transverse compression and out-of-plane shear. Compos Sci Technol 2008;68:829–39.

[28] Tang Z, Wang C, Yu Y. Failure response of fiber-epoxy unidirectional laminate under transverse tensile/compressive loading using finite-volume micromechanics. Compos B 2015;79:331–41.
[29] Ha SK, Jin KK, Huang Y. Micro-mechanics of failure (MMF) for continuous fiber reinforced composites. J Compos Mater 2008;42:1873–95.
[30] Fenner JS, Daniel IM. Testing the 2-3 shear strength of unidirectional composite. In: Thakre P, Singh R, Slipher G, editors. Mechanics of composite, hybrid and multifunctional materials. Conference proceedings of the society for experimental mechanics series. Springer; 2019.
[31] Dávila CG, Camanho PP, Rose CA. Failure criteria for FRP laminates. J Compos Mater 2005;39:323–45.
[32] Mesogitis TS, Skordos AA, Long AC. Uncertainty in the manufacturing of fibrous thermosetting composites: a review. Compos A 2014;57:67–75.
[33] Advani SG, Sozer M. Process modeling in composite manufacturing. 2nd ed. CRC Press; 2010.
[34] Aboudi J. Micromechanical analysis of the strength of unidirectional fiber composites. Compos Sci Technol 1988;33:79–96.
[35] Falcó O, Ávila RL, Tijs B, Lopes CS. Modelling and simulation methodology for unidirectional composite laminates in a Virtual Test Lab framework. Compos Struct 2018;190:137–59.
[36] Gopalakrishnan M, Muthu S, Subramanian R, Santhanakrishnan R, Karthigeyan LM. Tensile properties study of E-glass/epoxy laminate and π/4 quasi-isotropic E-glass/epoxy laminate. Polym Polym Compos 2016;24:429–46.
[37] Hsiao HM, Daniel IM. Effect of fiber waviness on stiffness and strength reduction of unidirectional composites under compressive loading. Compos Sci Technol 1996;56:581–93.
[38] Kaddour AS, Hinton MJ. Input data for test cases used in benchmarking triaxial failure theories of composites. J Compos Mater 2012;46:2295–312.
[39] Kaddour AS, Hinton MJ, Soden PD. Behaviour of ±45° glass/epoxy filament wound composite tubes under quasi-static equal biaxial tension-compression loading: experimental results. Compos B 2003;34:689–704.
[40] Kaddour AS, Hinton MJ, Smith PA, Li S. Mechanical properties and details of composite laminates for the test cases used in the third world-wide failure exercise. J Compos Mater 2013;47:2427–42.
[41] Namdar O, Darendeliler H. Buckling, postbuckling and progressive failure analyses of composite laminated plates under compressive loading. Compos B 2017;120:143–51.
[42] Soden PD, Hinton MJ, Kaddour AS. Lamina properties, lay-up configurations and loading conditions for a range of fibre-reinforced composite laminates. Compos Sci Technol 1998;58:1011–22.
[43] Perogamvros NG, Lampeas GN. Experimental and numerical investigation of AS4/8552 interlaminar shear strength under impact loading conditions. J Compos Mater 2015;50:2669–85.
[44] Reddy CV, Babu PR, Ramnarayanan R, Das D. Mechanical characterization of unidirectional carbon and glass/epoxy reinforced composites for high strength applications. Mater Today: Proc 2017;4:3166–72.
[45] Lee J, Soutis C. A study on the compressive strength of thick carbon fibre-epoxy laminates. Compos Sci Technol 2007;67:2015–26.
[46] Varandas LF, Arteiro A, Bessa MA, Melro AR, Catalanotti G. The effect of through-thickness compressive stress on mode II interlaminar crack propagation: a computational micromechanics approach. Compos Struct 2017;182:326–34.
[47] Chevalier J, Camanho PP, Lani F, Pardoen T. Multi-scale characterization and modelling of the transverse compression response of unidirectional carbon fiber reinforced epoxy. Compos Struct 2019;209:160–76.